

Maintenance and propagation of a deleterious mitochondrial genome by the mitochondrial unfolded protein response

Yi-Fan Lin¹, Anna M. Schulz¹, Mark W. Pellegrino¹, Yun Lu², Shai Shaham² & Cole M. Haynes^{1,3}

Mitochondrial genomes (mitochondrial DNA, mtDNA) encode essential oxidative phosphorylation (OXPHOS) components. Because hundreds of mtDNAs exist per cell, a deletion in a single mtDNA has little impact. However, if the deletion genome is enriched, OXPHOS declines, resulting in cellular dysfunction. For example, Kearns–Sayre syndrome is caused by a single heteroplasmic mtDNA deletion. More broadly, mtDNA deletion accumulation has been observed in individual muscle cells¹ and dopaminergic neurons² during ageing. It is unclear how mtDNA deletions are tolerated or how they are propagated in somatic cells. One mechanism by which cells respond to OXPHOS dysfunction is by activating the mitochondrial unfolded protein response (UPR^{mt}), a transcriptional response mediated by the transcription factor ATFS-1 that promotes the recovery and regeneration of defective mitochondria^{3,4}. Here we investigate the role of ATFS-1 in the maintenance and propagation of a deleterious mtDNA in a heteroplasmic *Caenorhabditis elegans* strain that stably expresses wild-type mtDNA and mtDNA with a 3.1-kilobase deletion (Δ mtDNA) lacking four essential genes⁵. The heteroplasmic strain, which has 60% Δ mtDNA, displays modest mitochondrial dysfunction and constitutive UPR^{mt} activation. ATFS-1 impairment reduced the Δ mtDNA nearly tenfold, decreasing the total percentage to 7%. We propose that in the context of mtDNA heteroplasmy, UPR^{mt} activation caused by OXPHOS defects propagates or maintains the deleterious mtDNA in an attempt to recover OXPHOS activity by promoting mitochondrial biogenesis and dynamics.

mtDNA mutations and deletions are relatively common within the mtDNA population of ageing post-mitotic cells but typically represent a minor percentage of the total mtDNA^{6,7}. However, if the deleterious mtDNA reaches a high enough percentage relative to wild-type mtDNA, it can, depending on the severity of the mtDNA lesion, become toxic and lead to disease⁸. As mtDNA encodes 13 (12 in *C. elegans*) essential components of the respiratory chain and ATP synthase, along with rRNAs and tRNAs required for their synthesis, an increase in deleterious heteroplasmy can perturb multiple cellular activities reliant on OXPHOS. However, the mechanism(s) that promote tolerance to large mtDNA deletions or contribute to their propagation are unknown.

Here we examine the role of the UPR^{mt} on the maintenance and propagation of a mtDNA with a 3.1 kb deletion (Δ mtDNA) encoding four essential OXPHOS genes (Fig. 1a) using a heteroplasmic *C. elegans* strain⁵. The UPR^{mt} is regulated by the transcription factor ATFS-1, which is normally efficiently imported into mitochondria and degraded. However, during mitochondrial stress or OXPHOS dysfunction, a percentage of ATFS-1 fails to be imported and traffics to the nucleus to activate a broad transcriptional program (over 500 transcripts) that promotes repair and recovery of mitochondrial function^{3,4}.

To examine the effect of Δ mtDNA on UPR^{mt} activation, Δ mtDNA was crossed into a transcriptional reporter worm harbouring the *hsp-6_{pr}::gfp* transgene used to monitor UPR^{mt} activation⁹. Consistent with previous studies demonstrating that perturbation of nuclear-encoded OXPHOS components activated the UPR^{mt} (Extended Data Fig. 1a)^{4,10}, Δ mtDNA also modestly activated the UPR^{mt}, which required *atfs-1* (Fig. 1b). Consistent with a previous report⁵, Δ mtDNA made up 60% of all mtDNAs (Fig. 1c). And, Δ mtDNA caused a significant reduction in basal oxygen consumption as well as total respiratory capacity (Fig. 1d), suggesting 60% Δ mtDNA perturbs OXPHOS and activates the UPR^{mt}.

Surprisingly, the development of worms harbouring Δ mtDNA was unaffected by RNAi-mediated knockdown of *atfs-1* (*atfs-1*(RNAi)), in stark contrast to worms with hypomorphic mutations in nuclear-encoded OXPHOS components (Fig. 1e)^{4,11}, indicating the UPR^{mt} is not required for development when the OXPHOS defect derives from a mtDNA deletion. Thus, we examined the effect of UPR^{mt} inhibition on Δ mtDNA levels by impairing several components required for *hsp-6_{pr}::gfp* induction^{4,12}. Notably, *atfs-1* deletion or knockdown caused a dramatic reduction in Δ mtDNA levels, shifting the percentage from 60% to 7% (Fig. 1c and Extended Data Fig. 1b–d), probably explaining the normal growth rate (Fig. 1e). Δ mtDNA quantification in individual wild-type or *atfs-1*-deletion worms was consistent with that observed in larger worm populations and in some cases Δ mtDNA was reduced below the limit of detection in worms lacking ATFS-1 (Extended Data Fig. 1e). Therefore, ATFS-1 and UPR^{mt} activation are required to maintain the deleterious mtDNA.

A mechanism by which deleterious mtDNA levels can be altered involves the germ-line bottleneck where only a small number of mtDNAs are passed maternally to the next generation, allowing shifts in heteroplasmy⁸. Because the *atfs-1*-deletion strain was generated via mating, it is unclear if the shift in Δ mtDNA occurred during germ-line transmission, somatic cell division and growth, or both. To examine the role of ATFS-1 in Δ mtDNA maintenance specifically in somatic cells, we employed *glp-4(bn2)* worms that lack germlines when raised at the restrictive temperature. Interestingly, exposure of worms to *atfs-1* RNAi from the L1 stage to adulthood also depleted Δ mtDNA relative to the identical worm population raised on control RNAi (Fig. 1f), consistent with a role for the UPR^{mt} in maintaining Δ mtDNA levels in post-mitotic somatic cells.

Because mitochondrial autophagy (mitophagy) could potentially eliminate Δ mtDNAs when *atfs-1* is inhibited, we examined the interaction between Δ mtDNA, *atfs-1* and known mitophagy components. Mitophagy involves the recognition of defective mitochondria by the kinase PINK-1. Once PINK-1 accumulates, it recruits the ubiquitin ligase Parkin (PDR-1 in *C. elegans*) to the mitochondrial outer membrane, which directs the damaged organelle to lysosomes for degradation¹³. As described previously, *pdr-1* deletion resulted in increased

¹Cell Biology Program, Memorial Sloan Kettering Cancer Center, New York, New York 10065, USA. ²Laboratory of Developmental Genetics, The Rockefeller University, New York, New York 10065, USA. ³BCMB Allied Program, Weill Cornell Medical College, 1300 York Avenue, New York, New York 10065, USA.

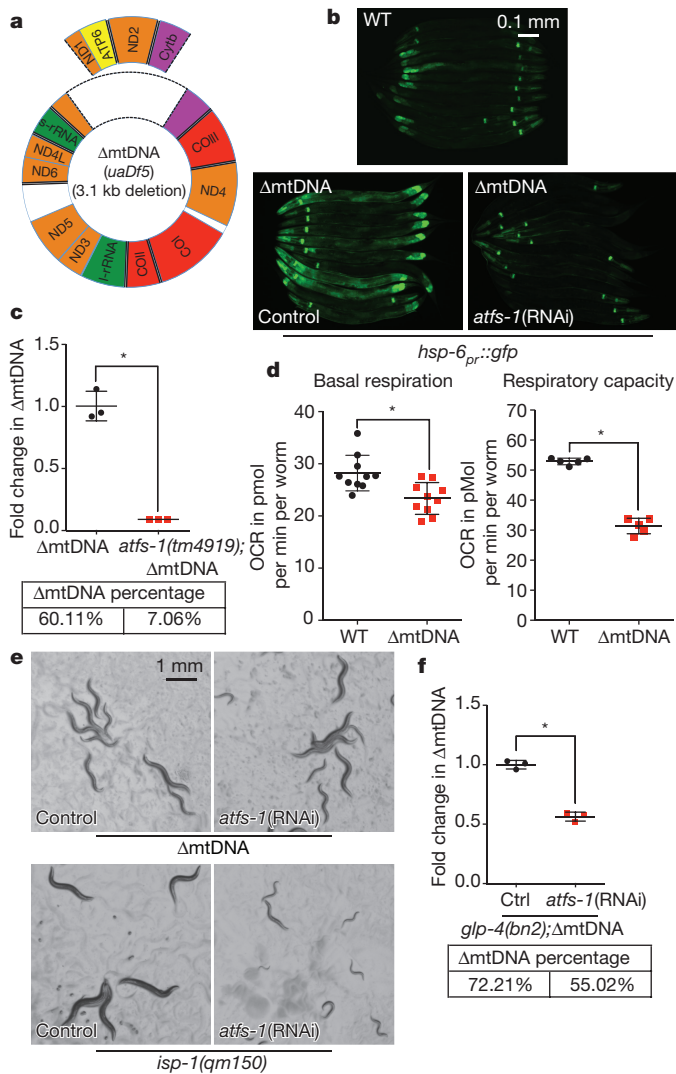


Figure 1 | ATFS-1 is required to maintain a deleterious mtDNA.

a, Comparison of wild-type and *uad5* deletion (Δ mtDNA) mtDNAs. **b**, *hsp-6_{pr}::gfp* in wild-type or Δ mtDNA worms on control or *atfs-1* RNAi. Scale bar, 0.1 mm. **c**, Δ mtDNA quantification as determined by qPCR in Δ mtDNA or *atfs-1(tm4919);* Δ mtDNA worms. $n = 3$; error bars, mean \pm s.d.; * $P < 0.03$ (Student's *t*-test). **d**, Oxygen consumption rates (OCR) in wild-type and Δ mtDNA worms. $n = 5$ and $n = 10$, respectively; error bars, mean \pm s.d.; * $P < 0.03$ (Student's *t*-test). **e**, Δ mtDNA or *isp-1(qm150)* worms raised on control or *atfs-1* RNAi. Scale bar, 1 mm. **f**, Δ mtDNA quantification as determined by qPCR in *glp-4(bn2);* Δ mtDNA worms on control or *atfs-1* RNAi. $n = 3$; error bars, mean \pm s.d.; * $P < 0.03$ (Student's *t*-test).

Δ mtDNA (Fig. 2a)¹⁴, consistent with mitophagy targeting defective mitochondria containing relatively high levels of deleterious mtDNAs¹⁵. However, the reduction of Δ mtDNA caused by *atfs-1* inhibition was only partially blocked by *pink-1;pdr-1* deletion or *atg-18* deletion, which impairs general autophagy (Fig. 2a and Extended Data Fig. 2a). Additionally, *atfs-1* inhibition did not impair development of *pink-1;pdr-1*-deficient Δ mtDNA worms (Fig. 2b) despite the increased UPR^{mt} activation (Fig. 2c). As PDR-1 inhibition did not completely restore Δ mtDNA in *atfs-1*-deletion worms, ATFS-1 probably promotes Δ mtDNA propagation independent of mitophagy or other Parkin-mediated activities¹⁶.

As modest UPR^{mt} activation was required to maintain the deletion genome (Fig. 1), we examined the effects of stronger UPR^{mt} activation on Δ mtDNA expansion or propagation. To further activate the UPR^{mt} in somatic cells, the mitochondrial protease SPG-7 was impaired by RNAi^{3,4} during development in worms lacking germlines.

Despite strong UPR^{mt} activation, Δ mtDNA levels did not increase (Fig. 2d and Extended Data Fig. 2b). However, because PINK-1 and Parkin are also activated by mitochondrial unfolded protein stress¹⁷, we wondered whether PINK-1 and PDR-1 activities limit Δ mtDNA accumulation. Remarkably, Δ mtDNA levels increased threefold in *pink-1;pdr-1*-deletion worms raised on *spg-7* RNAi (Fig. 2d) suggesting that UPR^{mt} activation can promote propagation of deleterious mtDNAs, which is antagonized by mitophagy during strong mitochondrial stress. However, because wild-type mtDNAs were also increased, the Δ mtDNA percentage was unaffected (Fig. 2d). As both wild-type and Δ mtDNA were increased by *spg-7*(RNAi), ATFS-1 may promote a mitochondrial biogenesis program in response to mitochondrial dysfunction. Notably, mitochondrial mass¹⁸ also increased in *pink-1;pdr-1*-deficient worms treated with *spg-7* RNAi (Fig. 2e) consistent with ATFS-1 mediating a compensatory mitochondrial biogenesis program that maintains Δ mtDNA. Combined, these results suggest that during strong mitochondrial stress, balanced PINK-1/PDR-1 and ATFS-1 activity limits Δ mtDNA accumulation.

To determine if ATFS-1 activation is sufficient to increase mitochondrial biogenesis and Δ mtDNAs independent of mitophagy, we used a mutant strain with constitutive UPR^{mt} activation owing to an amino acid substitution within the ATFS-1 mitochondrial targeting sequence¹⁹. Consistent with the UPR^{mt} promoting a mitochondrial biogenesis program, *atfs-1(et18)* animals also displayed a marked increase in the number of mitochondria (Fig. 3a). *atfs-1(et18)* worms also had increased Δ mtDNA and wild-type mtDNAs (Fig. 3b), however Δ mtDNA was further increased than wild-type mtDNAs, resulting in an increase of Δ mtDNA from 63% to 73%. Consistent with increased Δ mtDNAs, *atfs-1(et18);* Δ mtDNA worms developed slower than *atfs-1(et18)* worms (Fig. 3c) or Δ mtDNA worms⁵. And consistent with further OXPHOS impairment, *atfs-1(et18);* Δ mtDNA worms consumed less oxygen (Fig. 3d), had reduced mitochondrial

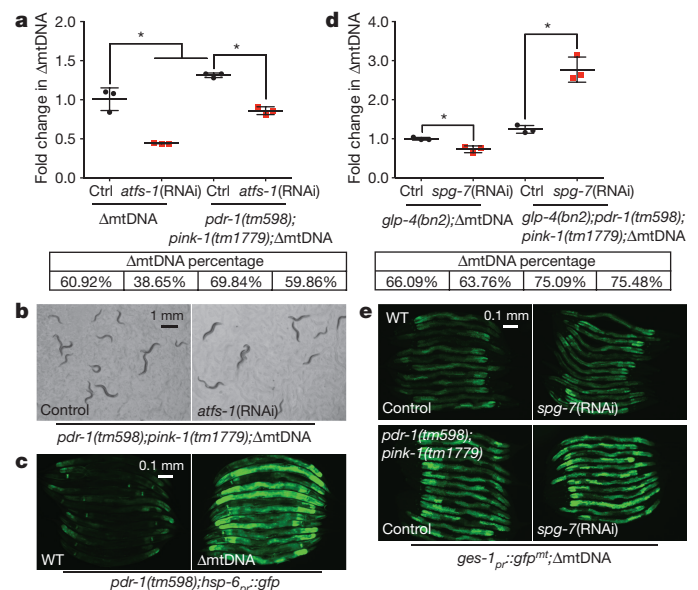


Figure 2 | ATFS-1 promotes Δ mtDNA maintenance and mitochondrial biogenesis largely independent of Parkin.

a, Δ mtDNA quantification as determined by qPCR in Δ mtDNA and *pdr-1(tm598);pink-1(tm1779);* Δ mtDNA worms raised on control or *atfs-1* RNAi. $n = 3$; error bars, mean \pm s.d.; * $P < 0.03$ (Student's *t*-test). **b**, *pdr-1(tm598);pink-1(tm1779);* Δ mtDNA worms raised on control or *atfs-1* RNAi. Scale bar, 1 mm. **c**, *pdr-1(tm598);hsp-6_{pr}::gfp* worms with wild-type or Δ mtDNA. Scale bar, 0.1 mm. **d**, Δ mtDNA quantification as determined by qPCR in *glp-4(bn2);* Δ mtDNA and *glp-4(bn2);pdr-1(tm598);pink-1(tm1779);* Δ mtDNA worms raised on control or *spg-7* RNAi. $n = 3$; error bars, mean \pm s.d.; * $P < 0.03$ (Student's *t*-test). **e**, *ges-1_{pr}::gfp^{mt};* Δ mtDNA or *ges-1_{pr}::gfp^{mt};pdr-1(tm598);pink-1(tm1779);* Δ mtDNA worms raised on control or *spg-7* RNAi. WT, wild type. Scale bar, 0.1 mm.

membrane potential (Extended Data Fig. 2c) and were sensitive to the OXPHOS inhibitor rotenone (Extended Data Fig. 2d). Combined, these results indicate that UPR^{mt} activation is detrimental in the presence of Δ mtDNAs.

To investigate potential causes of the OXPHOS deficiency and UPR^{mt} activation in Δ mtDNA worms, we compared expression of a gene within the Δ mtDNA deletion (*ND2*), that is only expressed by the population of wild-type mtDNAs, to mtDNA-encoded genes located outside of the deletion that are encoded by both wild-type and Δ mtDNAs (*ND4*, *ND6*) (Fig. 1a). Surprisingly, *ND2* transcripts were not reduced in Δ mtDNA or *atfs-1(et18);* Δ mtDNA animals despite the absence of the *ND2* gene in Δ mtDNA (Fig. 3e). Interestingly, *ND4* was expressed significantly more in both Δ mtDNA and *atfs-1(et18);* Δ mtDNA relative to wild-type worms while the nuclear-encoded complex I transcript *nuo-4* was unaffected (Fig. 3e). These

results suggest that mitochondrial dysfunction in Δ mtDNA worms is not due to reduction of transcripts encoded by genes within the mtDNA deletion.

Next, we performed electron microscopy to examine mitochondrial morphology in *atfs-1(et18)* harbouring 73% Δ mtDNA. The cristae were largely absent in these mitochondria (Fig. 3f), consistent with severe mitochondrial dysfunction and reduced OXPHOS (Fig. 3d). Notably, a number of autophagosome-like structures associated with degenerate mitochondria were observed only in *atfs-1(et18);* Δ mtDNA worms (Fig. 3f). And, consistent with increased mitophagy in *atfs-1(et18);* Δ mtDNA animals, *pdr-1* deletion further increased the percentage of Δ mtDNA (Fig. 3g). Combined, these results suggest that in the context of deleterious heteroplasmy, increased UPR^{mt} activation can further perturb mitochondrial function, potentially leading to increased mitophagy.

To better understand the ATFS-1-mediated transcriptional program that promotes Δ mtDNA maintenance and propagation, the transcriptomes of wild-type and *atfs-1(et18)* worms were examined. Activated ATFS-1 induced many transcripts suggestive of mitochondrial biogenesis, including the mitochondrial protein import machinery, the cardiolipin synthesis tafazzin, mitochondrial ribosome and translation factors, prohibitin complex components, mitochondrial chaperones and OXPHOS assembly factors (Supplementary Table 1), consistent with ATFS-1 regulating a mitochondrial biogenesis and mitochondrial proteostasis program to recover mitochondrial function. *atfs-1(et18)* also increased the mtDNA polymerase *polg-1*, the worm orthologue of the mtDNA-binding protein TFAM (*hmg-5*), as well as transcripts required for mitochondrial dynamics (Supplementary Table 1 and Extended Data Fig. 3a).

Interestingly, inhibition of mitochondrial fusion or fission by *fzo-1(RNAi)* or *drp-1(RNAi)* reduced the Δ mtDNA percentage in a similar manner to *atfs-1(RNAi)* (Fig. 3h) in Δ mtDNA worms, suggesting that organelle dynamics stimulated by the UPR^{mt} promote deleterious mtDNA maintenance. Because *fzo-1(RNAi)* inhibition had relatively little effect on mitochondrial biogenesis (Fig. 3a), only organelle morphology (Fig. 3a, lower panel), we speculate that organelle mixing mediated by *drp-1* and *fzo-1*, which requires OXPHOS function²⁰, limits the enrichment of deleterious mtDNAs in individual organelles and promotes tolerance to deleterious mtDNAs^{21,22}. Consistent with this idea, development of *atfs-1(et18);* Δ mtDNA animals was delayed when mitochondrial fusion was inhibited (Extended Data Fig. 3b). Impairment of *polg-1* and *hmg-5* also reduced the Δ mtDNA percentage in Δ mtDNA worms (Fig. 3h and Extended Data Fig. 3c), suggesting that replication and mtDNA protection is involved in maintaining the deleterious genome. Combined, these data suggest that through multiple outputs, ATFS-1 activation provides favourable conditions for Δ mtDNA proliferation.

These results suggest an unanticipated consequence of ATFS-1 and UPR^{mt} activation in the context of deleterious mtDNA heteroplasmy. While the UPR^{mt} is protective during exposure to mitochondrial toxins²³ or mutations within nuclear-encoded OXPHOS genes^{4,24}, in the context of mtDNA heteroplasmy, UPR^{mt} activation maintains the deleterious mtDNA. We propose that by inducing a mitochondrial recovery program, UPR^{mt} activation inadvertently propagates deleterious mtDNAs in an attempt to recover OXPHOS activity. These results potentially shed light on the underlying mechanisms that lead to mitochondrial diseases and the enrichment of Δ mtDNAs found in aged cells^{7,8}. They also emphasize the importance of UPR^{mt} regulation and suggest that prolonged UPR^{mt} activation is potentially harmful²⁵, as ATFS-1 activation creates an environment favourable for Δ mtDNAs.

Online Content Methods, along with any additional Extended Data display items and Source Data, are available in the online version of the paper; references unique to these sections appear only in the online paper.

Received 25 November; accepted 8 April 2016.

Published online 2 May 2016.

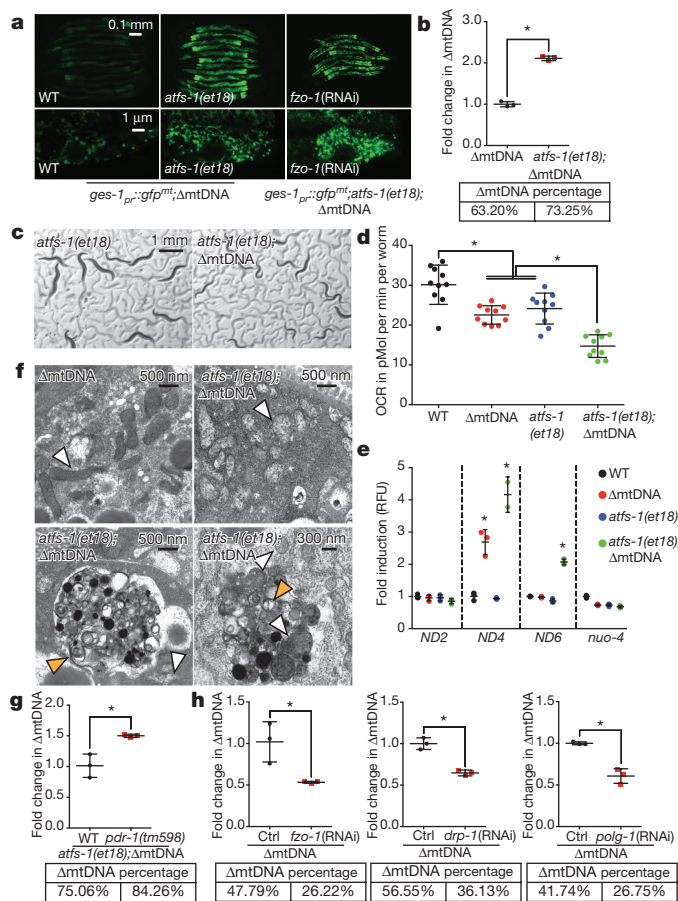


Figure 3 | ATFS-1 activation causes deleterious mtDNA expansion.

a, *ges-1_{pr}::gfp^{mt};* Δ mtDNA or *ges-1_{pr}::gfp^{mt};atfs-1(et18);* Δ mtDNA worms raised on control or *fzo-1* RNAi. The bottom panels are a single intestinal cell. WT, wild type. Scale bar, 0.1 mm (top) and 1 μ m (bottom).

b, Δ mtDNA quantification as determined by qPCR in Δ mtDNA or *atfs-1(et18);* Δ mtDNA worms. WT, wild type. $n = 3$; error bars, mean \pm s.d.; * $P < 0.03$ (Student's *t*-test).

c, Synchronized *atfs-1(et18)* and *atfs-1(et18);* Δ mtDNA worms. Scale bar, 1 mm. **d**, Oxygen consumption rates (OCR) of wild-type, Δ mtDNA, *atfs-1(et18)* and *atfs-1(et18);* Δ mtDNA worms. $n = 10$; error bars, mean \pm s.d.; * $P < 0.03$ (Student's *t*-test).

e, *ND2*, *ND4*, *ND6* and *nuo-4* transcripts as determined by qRT-PCR in wild-type, Δ mtDNA, *atfs-1(et18)* and *atfs-1(et18);* Δ mtDNA worms. $n = 3$; error bars, mean \pm s.d.; * $P < 0.03$ (Student's *t*-test). RFU, relative fluorescent units. **f**, An intestinal cell in Δ mtDNA and *atfs-1(et18);* Δ mtDNA worms. Mitochondria (white) and autophagosomes (orange) are indicated. Scale bars, 500 nm (lower right), 300 nm.

g, h, Δ mtDNA quantification as determined by qPCR in Δ mtDNA, *atfs-1(et18);* Δ mtDNA or *pdr-1(tm598);* Δ mtDNA worms raised on control, *fzo-1*, *drp-1*, or *polg-1* RNAi. $n = 3$; error bars, mean \pm s.d.; * $P < 0.03$ (Student's *t*-test).

1. Bua, E. *et al.* Mitochondrial DNA-deletion mutations accumulate intracellularly to detrimental levels in aged human skeletal muscle fibers. *Am. J. Hum. Genet.* **79**, 469–480 (2006).
2. Kraysberg, Y. *et al.* Mitochondrial DNA deletions are abundant and cause functional impairment in aged human substantia nigra neurons. *Nat. Genet.* **38**, 518–520 (2006).
3. Nargund, A. M., Fiorese, C. J., Pellegrino, M. W., Deng, P. & Haynes, C. M. Mitochondrial and nuclear accumulation of the transcription factor ATFS-1 promotes OXPHOS recovery during the UPR(mt). *Mol. Cell* **58**, 123–133 (2015).
4. Nargund, A. M., Pellegrino, M. W., Fiorese, C. J., Baker, B. M. & Haynes, C. M. Mitochondrial import efficiency of ATFS-1 regulates mitochondrial UPR activation. *Science* **337**, 587–590 (2012).
5. Tsang, W. Y. & Lemire, B. D. Stable heteroplasmy but differential inheritance of a large mitochondrial DNA deletion in nematodes. *Biochem. Cell Biol.* **80**, 645–654 (2002).
6. Greaves, L. C. *et al.* Clonal expansion of early to mid-life mitochondrial DNA point mutations drives mitochondrial dysfunction during human ageing. *PLoS Genet.* **10**, e1004620 (2014).
7. Taylor, S. D. *et al.* Targeted enrichment and high-resolution digital profiling of mitochondrial DNA deletions in human brain. *Ageing Cell* **13**, 29–38 (2014).
8. Stewart, J. B. & Chinnery, P. F. The dynamics of mitochondrial DNA heteroplasmy: implications for human health and disease. *Nat. Rev. Genet.* **16**, 530–542 (2015).
9. Yoneda, T. *et al.* Compartment-specific perturbation of protein handling activates genes encoding mitochondrial chaperones. *J. Cell Sci.* **117**, 4055–4066 (2004).
10. Durieux, J., Wolff, S. & Dillin, A. The cell-non-autonomous nature of electron transport chain-mediated longevity. *Cell* **144**, 79–91 (2011).
11. Baker, B. M., Nargund, A. M., Sun, T. & Haynes, C. M. Protective coupling of mitochondrial function and protein synthesis via the eIF2 α kinase GCN-2. *PLoS Genet.* **8**, e1002760 (2012).
12. Haynes, C. M., Petrova, K., Benedetti, C., Yang, Y. & Ron, D. ClpP mediates activation of a mitochondrial unfolded protein response in *C. elegans*. *Dev. Cell* **13**, 467–480 (2007).
13. Narendra, D. P. *et al.* PINK1 is selectively stabilized on impaired mitochondria to activate Parkin. *PLoS Biol.* **8**, e1000298 (2010).
14. Valenci, I., Yonai, L., Bar-Yaacov, D., Mishmar, D. & Ben-Zvi, A. Parkin modulates heteroplasmy of truncated mtDNA in *Caenorhabditis elegans*. *Mitochondrion* **20**, 64–70 (2015).
15. Suen, D. F., Narendra, D. P., Tanaka, A., Manfredi, G. & Youle, R. J. Parkin overexpression selects against a deleterious mtDNA mutation in heteroplasmic cybrid cells. *Proc. Natl Acad. Sci. USA* **107**, 11835–11840 (2010).
16. Scarffe, L. A., Stevens, D. A., Dawson, V. L. & Dawson, T. M. Parkin and PINK1: much more than mitophagy. *Trends Neurosci.* **37**, 315–324 (2014).
17. Jin, S. M. & Youle, R. J. The accumulation of misfolded proteins in the mitochondrial matrix is sensed by PINK1 to induce PARK2/Parkin-mediated mitophagy of polarized mitochondria. *Autophagy* **9**, 1750–1757 (2013).
18. Palikaras, K., Lionaki, E. & Tavernarakis, N. Coordination of mitophagy and mitochondrial biogenesis during ageing in *C. elegans*. *Nature* **521**, 525–528 (2015).
19. Rauthan, M., Ranji, P., Aguilera Pradenas, N., Pitot, C. & Pilon, M. The mitochondrial unfolded protein response activator ATFS-1 protects cells from inhibition of the mevalonate pathway. *Proc. Natl Acad. Sci. USA* **110**, 5981–5986 (2013).
20. Mishra, P., Carelli, V., Manfredi, G. & Chan, D. C. Proteolytic cleavage of Opa1 stimulates mitochondrial inner membrane fusion and couples fusion to oxidative phosphorylation. *Cell Metab.* **19**, 630–641 (2014).
21. Chen, H. *et al.* Mitochondrial fusion is required for mtDNA stability in skeletal muscle and tolerance of mtDNA mutations. *Cell* **141**, 280–289 (2010).
22. Nakada, K. *et al.* Inter-mitochondrial complementation: Mitochondria-specific system preventing mice from expression of disease phenotypes by mutant mtDNA. *Nat. Med.* **7**, 934–940 (2001).
23. Pellegrino, M. W. *et al.* Mitochondrial UPR-regulated innate immunity provides resistance to pathogen infection. *Nature* **516**, 414–417 (2014).
24. Schieber, M. & Chandel, N. S. TOR signaling couples oxygen sensing to lifespan in *C. elegans*. *Cell Reports* **9**, 9–15 (2014).
25. Lamech, L. T. & Haynes, C. M. The unpredictability of prolonged activation of stress response pathways. *J. Cell Biol.* **209**, 781–787 (2015).

Supplementary Information is available in the online version of the paper.

Acknowledgements We thank B. Lemire, the National Bioresource Project and the *Caenorhabditis* Genetics Center for providing *C. elegans* strains (funded by NIH Office of Research 362 Infrastructure Programs (P40 OD010440), and the Genomics and Bioinformatics Facilities at Memorial Sloan Kettering Cancer Center). This work was supported by National Institutes of Health grants (R01AG040061 and R01AG047182) to C.M.H. and (R01HD078703 and R01NS081490) to S.S., and a Parkinson's Disease Foundation grant (PDF-FBS-1314) to Y.-F.L. and Deutsche Forschungsgemeinschaft (DFG, SCHU 3023/1-1) to A.M.S.

Author Contributions Y.-F.L. and C.M.H. planned the experiments. Y.-F.L. generated the worm strains and performed the mtDNA quantification and obtained the images. A.M.S. and Y.-F.L. performed the oxygen consumption analysis and M.W.P. performed the microarray experiments. Electron microscopy was performed by Y.Lu under the supervision of S.S. Y.-F.L. and C.M.H. wrote the manuscript.

Author Information The microarray data have been deposited in a MIAME-compliant format to the Gene Expression Omnibus database under accession number GSE73669. Reprints and permissions information is available at www.nature.com/reprints. The authors declare no competing financial interests. Readers are welcome to comment on the online version of the paper. Correspondence and requests for materials should be addressed to C.M.H. (haynesc@mskcc.org).

METHODS

Worm strains, staining and rotenone treatment. The *atfs-1(tm4919)*, *pink-1(tm1779)* and *pdr-1(tm598)* strains were obtained from the National BioResource Project (Tokyo, Japan) and the N2 (wild-type mtDNA), LB138 (*uaDf5* or Δ mtDNA), *atg-18(gk378)*, *isp-1(qm150)* and *glp-4(bn2)* strains from the *Caenorhabditis* Genetics Center (Minneapolis, Minnesota). The *atfs-1(et18)* strain was a gift from M. Pilon. The *ges-1_{pr}::gfp^{mt}* worms used for visualizing mitochondrial content and the reporter strain *hsp-6_{pr}::gfp* for visualizing UPR^{mt} activation have been described^{9,23}. Hermaphrodites were used for all experiments. Rotenone treatment and TMRE staining was performed by synchronizing and raising worms on plates previously soaked with M9 buffer containing rotenone (Tocris), DMSO, or TMRE (Molecular Probes). TMRE-stained worms were subsequently placed on control plates to remove TMRE-containing bacteria in the digestive tract for 3 h before imaging.

mtDNA quantification. Wild-type mtDNA and Δ mtDNA quantification was performed using qPCR-based methods similar to previously described assays^{14,26}. 20–30 worms were collected in 30 μ l of lysis buffer (50 mM KCl, 10 mM Tris-HCl (pH 8.3), 2.5 mM MgCl₂, 0.45% NP-40, 0.45% Tween 20, 0.01% gelatin, with freshly added 200 μ g ml⁻¹ proteinase K) and frozen at -80°C for 20 min before lysis at 65°C for 80 min. Relative quantification was used for determining the fold changes in mtDNA between samples. 1 μ l of lysate was used in each triplicate qPCR reaction. qPCR was performed using the Thermo-Scientific SyBr Green Maxima Mix and the MyiQ2 Two-Colour Real-Time PCR Detection System (Bio-Rad Laboratories). Primers that specifically amplify wild-type or Δ mtDNA are listed in Supplementary Table 2. Primers that amplify a non-coding region near the nuclear-encoded *ges-1* gene were used as a control (Supplementary Table 2).

Absolute quantification was also performed to determine the percentage or ratio of Δ mtDNA relative to total mtDNA (Δ mtDNA and wild-type mtDNA). This approach was also employed to determine Δ mtDNA number per nuclear genome in the individual worm analysis. Standard curves for each qPCR primer set were generated using purified plasmids individually containing approximately 1 kb of the mtDNA or nuclear DNA sequence specific for each primer set^{14,26}. The concentration of the purified plasmids was determined using a Nanodrop spectrometer (Thermo Scientific). mtDNA was harvested from synchronized worms at the L4 stage. For the experiments involving the *glp-4(bn2)* strain, worms were raised at 25°C and harvested 3 days after hatching. All qPCR results are presented as technical replicates, but each experiment has been repeated three or more times. A Student's *t*-test was employed to determine the level of statistical significance.

RNA isolation and qRT-PCR analysis. Worms were synchronized and raised in liquid culture until the L4 stage when they were harvested and compacted into pellets on ice. Total RNA was extracted from a 30–50 μ l worm pellet using RNA STAT (Tel-Test). For the analysis of mtDNA-encoded mRNAs, the RNA extracts were then treated with DNase using the DNA-free kit (Ambion) to reduce mtDNA contamination. 1 μ g of RNA was used for synthesizing cDNA with the iScript cDNA Synthesis Kit (Bio-Rad Laboratories). qPCR was performed using the Thermo-Scientific SyBr Green Maxima Mix and the MyiQ2 Two-Colour Real-Time PCR Detection System (Bio-Rad Laboratories). Primer sequences are listed in Supplementary Table 2. All qPCR results are presented as technical replicates,

but each experiment has been repeated three or more times. A Student's *t*-test was employed to determine the level of statistical significance.

Statistics. All experiments were performed three times yielding similar results and comprised of biological replicates. The sample size and statistical tests were chosen based on previous studies with similar methodologies and the data met the assumptions for each statistical test performed. No statistical method was used in deciding sample sizes. No blinded experiments were performed and randomization was not used. For all figures, the mean \pm standard deviation (s.d.) is represented unless otherwise noted.

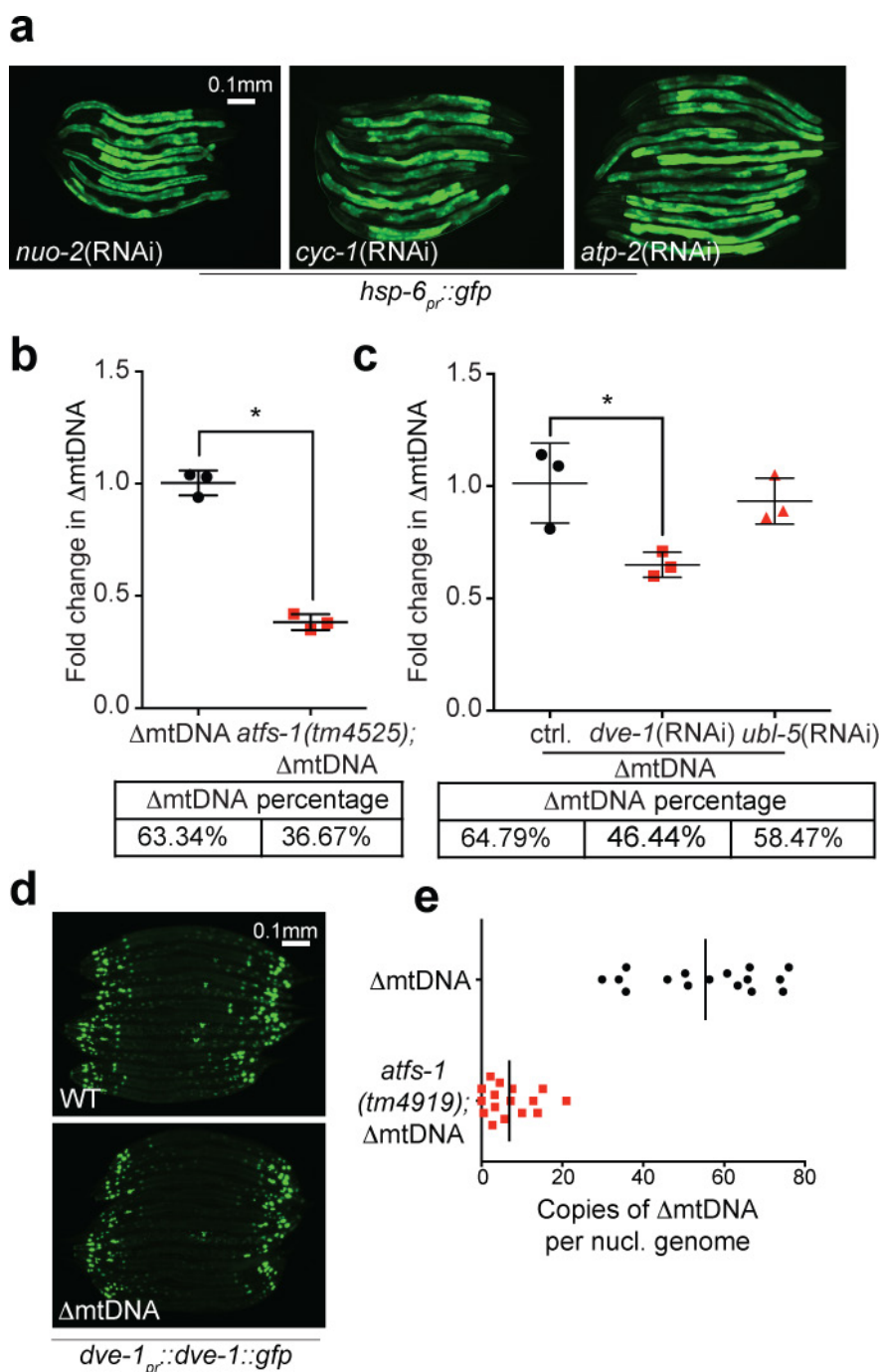
Imaging. Whole-worm images were obtained using either a Zeiss AxioCam MRm camera mounted on a Zeiss Imager Z2 microscope or a Zeiss M2BIO dissecting scope. Exposure times were the same within each experiment. Fluorescent (*ges-1_{pr}::gfp^{mt}*) mitochondrial morphology images of the most proximal intestinal cells were taken with a Nikon Eclipse Ti confocal microscope. The signal intensity of each image was adjusted to highlight the differences in mitochondrial morphology as opposed to mitochondrial density. All images are representative of more than three images.

Electron microscopy. Animals were prepared for electron microscopy using standard methods²⁷. Ultrathin serial sections (80 nm) were collected using a Leica Ultracut UCT Ultramicrotome. Sections at two levels, 100 μ m and 110 μ m away from the head region, for each genotype were examined. Electron microscopy images were acquired using a FEI Tecnai G2 Spirit BioTwin transmission electron microscope operating at 120 kV with a Gatan 4K \times 4K digital camera.

Microarray analysis. Wild-type (N2) and *atfs-1(et18)* worms were synchronized by bleaching, and harvested at the L4 stage of development. Total RNA was extracted using the RNA STAT reagent (Tel-Test) and used for double-stranded cDNA synthesis using the iScript cDNA Synthesis Kit (Bio-Rad Laboratories). Microarray analysis using GeneChip *C. elegans* genome arrays (Affymetrix) was conducted as previously described⁴. Differences in gene expression between wild-type and *atfs-1(et18)* worms was determined using Anova streamlined (Partek Genomic Suite (v6.5)). Supplementary Table 1 contains the relative fold induction and *P* values for each mRNA. Confirmation of the microarray results was performed via qRT-PCR as described⁴. Primers are listed in Supplementary Table 2.

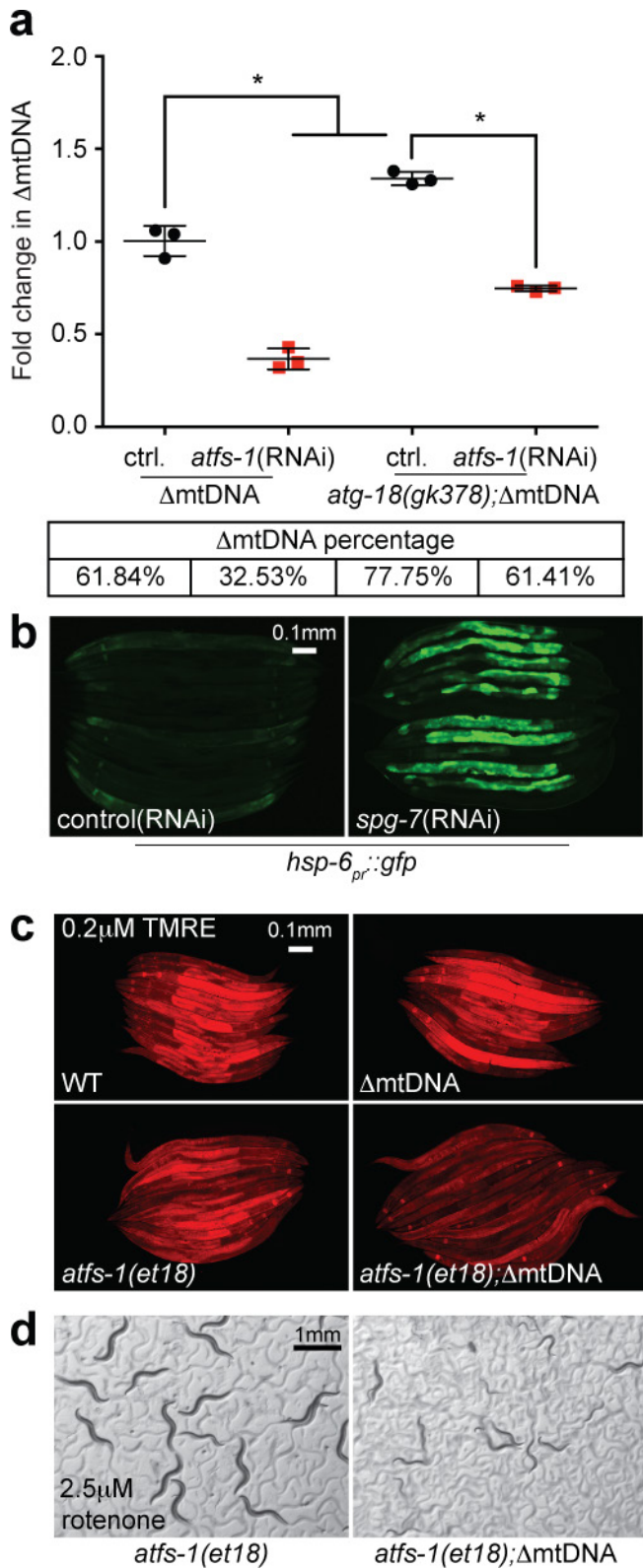
Oxygen consumption. Oxygen consumption was measured using a Seahorse XF96 Analyzer at 25°C similar to that described previously²⁸. In brief, adult worms were transferred onto empty plates and allowed to completely digest the remaining bacteria for 1 h, after which four worms were transferred into each well of a 96-well microplate containing 200 μ l M9 buffer. Basal respiration was measured for a total of 60 min, in 6-min intervals that included a 2 min mix, a 2 min time delay and a 2 min measurement. To measure respiratory capacity, 15 μ M FCCP was injected, the OCR (oxygen consumption rate) reading was allowed to stabilize for 15 min then measured for five consecutive intervals. Each measurement was considered one technical replicate.

26. He, L. *et al.* Detection and quantification of mitochondrial DNA deletions in individual cells by real-time PCR. *Nucleic Acids Res.* **30**, e68 (2002).
27. Bargmann, C. I., Hartwig, E. & Horvitz, H. R. Odorant-selective genes and neurons mediate olfaction in *C. elegans*. *Cell* **74**, 515–527 (1993).
28. Andreux, P. A. *et al.* A method to identify and validate mitochondrial modulators using mammalian cells and the worm *C. elegans*. *Sci. Rep.* **4**, 5285 (2014).

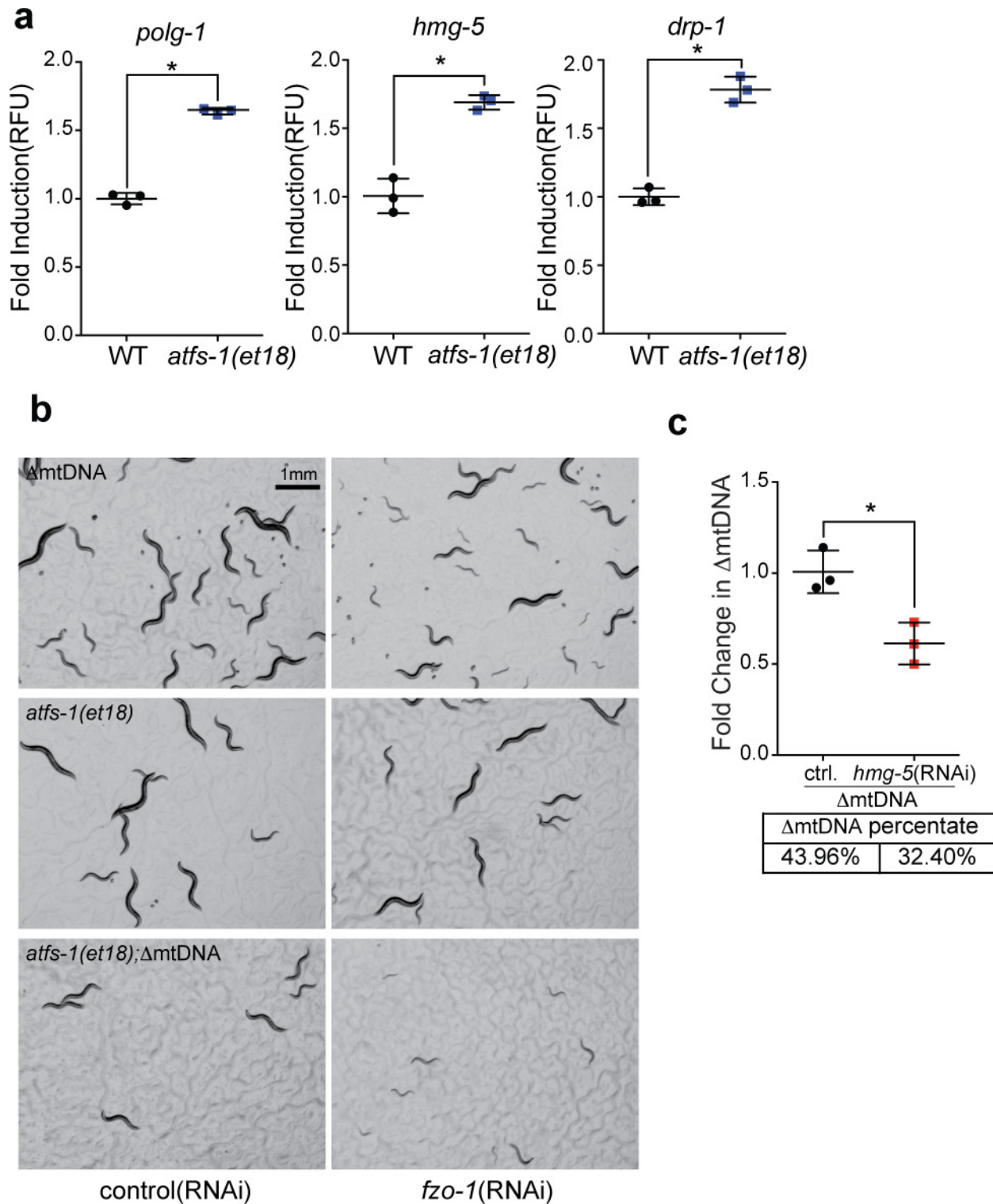


Extended Data Figure 1 | RNAi of nuclear encoded OXPHOS components activates the UPR^{mt}, and UPR^{mt} signalling components are required for Δ mtDNA propagation. **a**, Images of *hsp-6_{pr}::gfp* worms raised on *nuo-2* (complex I), *cyc-1* (cytochrome *c*) or *atp-2* (complex V) RNAi. Scale bar, 0.1 mm. **b**, Relative Δ mtDNA quantification as determined by qPCR in Δ mtDNA or *atfs-1(tm4525);* Δ mtDNA worms. *n* = 3; error bars, mean \pm s.d.; **P* < 0.03 (Student's *t*-test). **c**, Relative

Δ mtDNA quantification as determined by qPCR in Δ mtDNA worms raised on control, *dve-1*, or *ubl-5* RNAi. *n* = 3; error bars, mean \pm s.d.; **P* < 0.03 (Student's *t*-test). **d**, Images of *dve-1_{pr}::dve-1::gfp* in wild-type or Δ mtDNA worms. Scale bar, 0.1 mm. **e**, Ratios of Δ mtDNA and nuclear genomic DNA as determined by qPCR in individual Δ mtDNA and *atfs-1(tm4919);* Δ mtDNA worms. Black bars represent the mean. *n* = 16; mean *P* < 0.0001 (Student's *t*-test).



Extended Data Figure 2 | The reduction in Δ mtDNA caused by *atfs-1*(RNAi) is largely independent of autophagy, and ATFS-1 activation in the presence of a deleterious mtDNA is harmful.
a, Relative Δ mtDNA quantification as determined by qPCR in Δ mtDNA and *atg-18(gk378);ΔmtDNA* worms raised on control or *atfs-1* RNAi. $n = 3$; error bars, mean \pm s.d.; * $P < 0.03$ (Student's *t*-test). **b**, Images of *hsp-6_{pr}::gfp* worms raised on control or *spg-7* RNAi. Scale bar, 0.1 mm. **c**, Images of TMRE-stained wild-type, Δ mtDNA, *atfs-1(et18)* and *atfs-1(et18);ΔmtDNA* worms. Scale bar, 0.1 mm. **d**, Images of synchronized *atfs-1(et18)* and *atfs-1(et18);ΔmtDNA* worms raised on 2.5 μ M rotenone 4 days after hatching. Scale bar, 1 mm.



Extended Data Figure 3 | *polg-1*, *hmg-5* and *drp-1* mRNAs are induced in *atfs-1(et18)* worms, and mitochondrial fusion is required for the development of *atfs-1(et18)* worms harbouring Δ mtDNA. a, *polg-1*, *hmg-5* and *drp-1* transcripts as determined by qRT-PCR in wild-type and *atfs-1(et18)* worms. $n = 3$; error bars, mean \pm s.d.; * $P < 0.03$ (Student's

t-test). RFU, random fluorescent units. b, Images of synchronized Δ mtDNA, *atfs-1(et18)*, and *atfs-1(et18);* Δ mtDNA worms raised on control or *fzo-1* RNAi. Scale bar, 1 mm. c, Δ mtDNA quantification as determined by qPCR in Δ mtDNA worms raised on control or *hmg-5* RNAi. $n = 3$; error bars, mean \pm s.d.; * $P < 0.03$ (Student's *t*-test).